Line-shaped Convective Band Developed Over the Osaka Plain

Hiromu SEKO[*1], Yoshimasa, KUMAHARA[2], Kazuo SAITO[1]
[1] Meteorological Research Institute, Japan Meteorological Agency, Tsukuba, Japan
[2] Osaka District Meteorological Observatory, Japan Meteorological Agency, Osaka, Japan

1. Introduction

Heavy rainfalls are often caused by line-shaped bands when the moving speed of the bands is slow. Therefore, the study on the structure and evolution of the line-shaped bands is important for the disaster prevention.

The line-shaped band, which is referred to as 'Yodogawa-Channel' (YC), frequently occurs over the Osaka plain. Although the line-shaped bands at Kyushu and Sea of Japan have been investigated by using the Radar data and outputs of the numerical model, the structure and evolution of the YC was not fully investigated so far. In this study, the precipitation distribution is compared with the observed one, and then the structure and moving speed of the band is investigated using the outputs of the numerical models.

2. Evolution of the line-shaped band

Left panels of fig. 1 show the precipitation distributions observed by conventional radars. On 4 April 2003, the low pressure was located at the Sea of Japan and the cold front extended southward from the low pressure (not shown). The large precipitation area **A** extended from north-northeast to south-southwest in fig. 1 was associated with the cold front. Along **A**, the southerly flow from the south of the band was converged with the southwesterly flow from the west (not shown). After the precipitation band **A** moved eastward, the short convective band **B**, which is 'Yodogawa-Channel' band, was generated at 12JST (Japan Standard tome, 9JST corresponds to 0UTC). This convective band **B** stayed until 14JST, and then began to decay and bend southeastward. Another convective band **C** was generated on the west of **B** at 12JST. The band **C** was generated on the convergence line of aforementioned southwesterly flow and westerly flow on the west of **C**. The surface temperature behind **B** was cold, while the temperature between **A** and **C** was similar to that on the east of **A** (not shown). The local low- and high-pressures were observed at front of and in the intense precipitation regions in **A** (not shown).

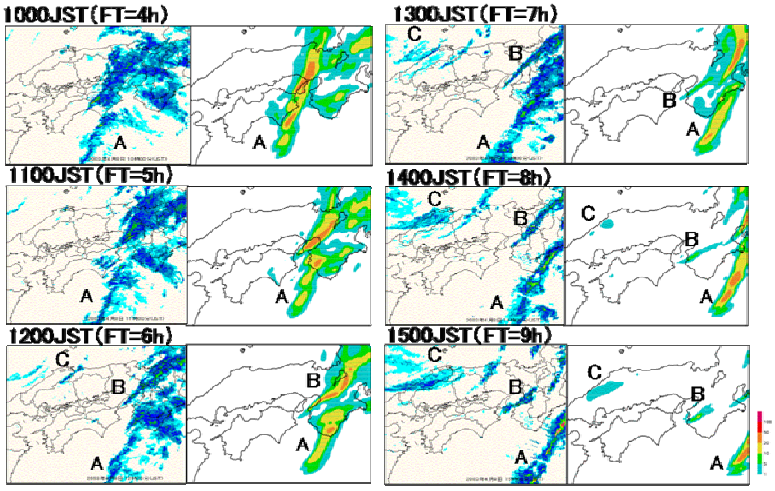

Fig.1 Observed precipitation regions from 10JST to 15JST on 8 April, 2003 and the precipitation simulated by JMANHM.

These convective bands were simulated by JMANHM (Saito et al, 2001) with the horizontal grid interval of 5 km. The simulated distribution of the precipitation was similar to the observed one, although the bending of the band **B** was earlier and **C** was weaker (right panels of fig. 1). Because the aforementioned features of the temperature and pressure distribution were also well reproduced (not shown), the structure of the convective band is explained in the next section.

3. Structure of the YC band

The convective band was simulated by JMANHM with a grid interval of 2 km. The initial and boundary data were produced by spatial and temporal interpolations. The evolution of the convective band **B** from 1150JST to 1310JST and the 3-dimensional structure at 1230JST are shown in figs. 2 and 3, respectively. The line-shaped band was bended southeastward at 1230JST, and then split into the southern part (**BS**) and northern part (**BN**) at 1310JST. The reason of the difference of the speed is explained in the section 4.

Along **BS**, the low-level southerly flow between **A** and **BS** was warm and humid (figs. 3a and 3c). This low-level inflow was converged with the westerly flow and ascended (fig. 3d). The westerly flow originated from the Sea of Setonai-kai on the west of **B** (fig.2). This westerly flow also intruded into the eastern edge of **BN** and lifted up the southerly flow on the east of **A** (fig. 3d). The temperature under **BN** was cold, because of the evaporation of the rain water (fig. 3c). In front of **BN**, a low pressure area existed (fig. 3e). Because the low pressure area moved with **BN**, this low-pressure is deduced to be produced by the release of the latent heat at the middle level. On the other hand, a high pressure area was produced in the precipitation area **BN** due to the evaporation of the rain water. At the height of 3 km, southwesterly flow, whose direction was parallel to the band, was dominant (fig. 3b). It is noted that there were no large descending areas near the band (fig. 2d). Namely, the

* hseko@mri-jma.go.jp, phone +81-29-853-8640; fax +81-29-853-8649

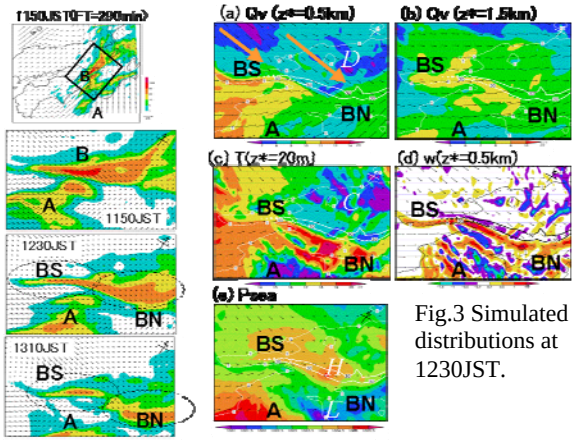

Fig.2 Simulated precipitation at 1150-1310JST.

Fig.3 Simulated distributions at 1230JST.

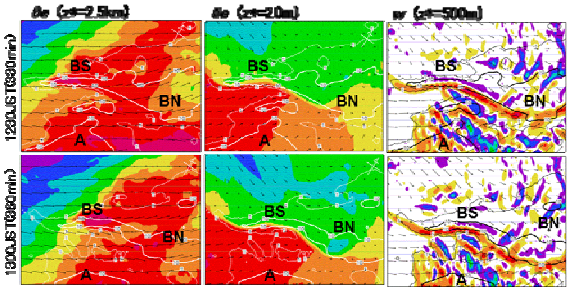

Fig.4 θe and vertical velocity distribution at 1230JST and 1300JST. Counter lines indicates the precipitation regions.

surface cold pool was generated by the low-level westerly flow and the mechanism that the middle-level dry air enhances convection did not work in this case. These features indicate that this band was back-and-side-building type (Seko and Nakamura, 2002).

4. Development of decay of the YC band

Next, the development and decay of **B** is explained. As mentioned before, the southerly flow between **A** and **B** generated **B**. When the time variation of wind speed of southerly flow was monitored, the wind speed was increased due to the low-pressure at the front of the intense precipitation region, and then decreased after **B** was generated (not shown). The convective band **B** did not increase the wind speed of the southerly flow. Therefore, the monitoring of the southerly flow before the generation of **B** is important for the prediction of YC band. Figure 4 shows the equivalent potential temperature (θe) distribution when the band **B** was decaying. At 1300JST, the low-θe air expanded over the southern tip of **B** (right panels in fig. 3) and the updraft there was weakened, although the southerly inflow changed slightly. This evolution indicates that the middle-level dry air weakened the convective band **B**.

4. Moving speed of YC band

As mentioned in section 2, the moving speed of **BN** was faster than that of **BS**. In this section, the difference of the moving speeds is discussed. Firstly, the surface horizontal wind and pressure within the rectangle in fig.5 were averaged, and then averaged value was substituted into eq.(2),

$$-(v-V)\frac{\partial(v-V)}{\partial y}-\frac{1}{\rho}\frac{\partial p}{\partial y}+F_y=\frac{\partial v}{\partial t}\,(=0:\textit{assumption}) \quad (1),$$

$$\int_a^b F_y dy=\tfrac{1}{2}v^2\Big|_a^b-V v\Big|_a^b+\frac{1}{\rho}p\Big|_a^b \quad (2),$$

$$V=\left(\frac{1}{2}v^2\Big|_a^b+\frac{1}{\rho}p\Big|_a^b-\int_a^b F_y dy\right)\Big/v\Big|_a^b \quad (3)$$

where V is the moving speed of the band and F is the residual terms. It is expected that F was composed of the friction and Colrolis force terms; the function of the wind velocity. Thus, F was estimated as a function of horizontal wind velocity and substituted to (3). Because the estimated speed was roughly close to the simulated one (fig. 7), the contributions of the advection term, pressure gradient force term and residual term were plotted in fig. 8. In **BN**, the pressure gradient force moved the band eastward and other terms disturbed the movement. On the contrary in **BS**, F moved the band eastward.

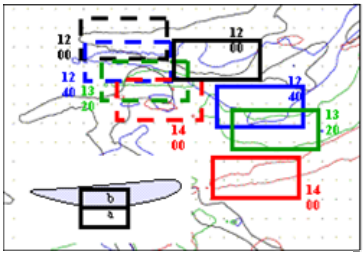

Fig. 6 Movement of the northern and southern parts of the line-shaped band.

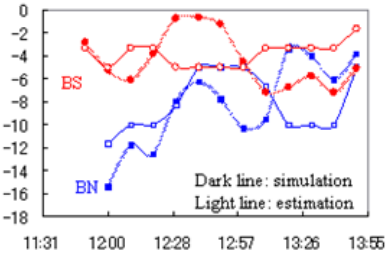

Fig.7 Simulated and estimated moving speed of the northern and southern parts of the line-shaped band.

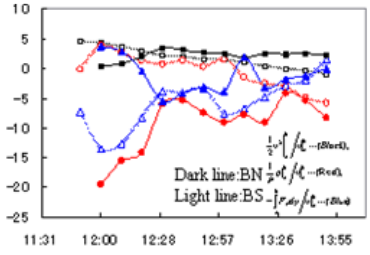

Fig. 8 Contributions of advection, pressure gradient and other terms on the moving speed of the line-shaped band.

References

Saito, K. T. Kato, H. Eito, and C. Muroi, 2001: Documentation of the Meteorological Research Institute/Numerical Prediction Division Unified Nonhydrostatic Model. *Tech, Rep. of the MRI*, **42**, p133.

Seko, H., and H. Nakamura, 2002: Numerical study of the shape and maintenance mechanisms of meso-β scale line shaped precipitation system in the middle-latitude, *CAS/JSC WGNE Research Activities in Atmospheric and Oceanic Models*,**33**,5-30.